

# Effective exponents for the diffusive coarsening of wet foams and analogous materials

Douglas J. Durian<sup>1,2</sup>

<sup>1</sup>*Department of Physics and Astronomy, University of Pennsylvania, Philadelphia, PA 19104, USA*

<sup>2</sup>*Center for Computational Biology, Flatiron Institute,  
Simons Foundation, New York, NY 10010, USA*

(Dated: June 30, 2023)

Empirical exponents for the growth of average domain size commonly lie between the known limits of 1/2 and 1/3. Here, a framework is developed in the context of foams to quantitatively explain such intermediate exponents, based on a model of gas diffusion and microstructure in which bubbles are approximately spherical and meet at approximately circular films. This predicts growth that is only logarithmically different from a 1/3 power law for nearly-kissing spheres at jamming. It also predicts how the growth law and effective exponents vary with liquid content, as set by the film radius. These predictions compare well with experimental data for two different foaming systems.

Approximate power-law growth of average domain size as  $R \sim t^\beta$  is encountered in a wide range of natural and engineered phase-separating materials, ranging from bubbles and droplets in fluid systems like foams and emulsions to grains in solid systems like metallic alloys [1–3]. It arises from the tendency of the domain size and topology distributions to evolve into statistically self-similar scaling states, where distribution shapes and dimensionless moment ratios are time-independent [1]. This allows prediction of exponents in certain limits. Canonical examples include compressed grains and very dry foams, where domains essentially fill space [3–10], and very dilute droplets or grains where the interstitial medium nearly fills space [2, 11–13]. The former behaves as  $R \sim t^{1/2}$  while the latter behaves as  $R \sim t^{1/3}$ .

Actual materials usually fall between these extremes, and many works have addressed how rate constants change away from both the “dilute grain” [2, 14] and the “compressed grain / dry foam” [15–19] limits, assuming fixed exponents. But it is also common to analyze data in terms of variable growth exponents,  $\beta$  [20–22]. *E.g.* for the case of foams,  $\beta$  was found to have a sigmoidal crossover from 1/2 in the dry limit to 1/3 at the unjamming limit of about 36% liquid [21]. It is very puzzling that this crossover came to completion at the jamming transition, rather than at the expected dilute-bubble limit of 100% liquid. The urgency of understanding exponent behavior is increased by newer experiments aboard the International Space Station (ISS) [23–25], where wet foams of variable liquid content can coarsen for extended duration without gravitational drainage of the foaming solution. The purpose of this paper is to provide a theoretical framework for understanding the variation of coarsening exponents between the limits where  $\beta = 1/2$  and  $1/3$  firmly hold. While this is developed in the particular context of wet foams, it also applies to broader classes of materials like emulsions and alloys with analogous microstructure.

To begin, power laws for average bubble growth in coarsening foams can be understood in the dry and wet limits as follows. In both cases it is driven by a charac-

teristic Laplace pressure difference, which gives a characteristic amplitude for the dissolved gas concentration gradient between neighboring bubbles as  $\Delta\phi \propto h\sigma/R$  where  $h$  is Henry’s constant,  $\sigma$  is surface tension, and  $R$  is an average sphere-equivalent bubble radius. Gas diffuses down this gradient, from smaller bubbles toward larger bubbles, causing average growth and a reduction in total interfacial area. This gives the average volumetric growth rate from Fick’s law as  $dR^d/dt \propto R^{d-1}(D\Delta\phi/L)$  where  $d$  is dimensionality,  $L$  is the characteristic distance over which the gas concentration gradient exists, and  $D$  is the dissolved gas diffusivity. For very dry foams  $L$  equals film thickness,  $\ell$ , while for dilute bubbles very far apart it equals  $R$ . The latter is based on solution of the diffusion equation for the radial concentration field around an isolated spherical bubble, decaying asymptotically to a value reflecting the mean from all the bubbles [11–13]. These ingredients combine to give an average growth law of  $dR/dt \propto R^{1-1/\beta}$ , independent of dimensionality, where  $\beta$  is 1/2 in the dry limit and 1/3 in the wet limit. Separating variables and integrating gives

$$R(t) = [\mathcal{D}(t - t_o) + R_o^{1/\beta}]^\beta \quad (1)$$

where  $\mathcal{D}$  is a materials constant times a numerical factor reflecting interplay of bubble size and contact number distributions [3, 26, 27] and the integration constants are such that  $R_o$  is the characteristic bubble radius at time  $t_o$ . Eq. (1) presumes that the system is in a self-similar scaling state. If not, the decay of transients on approach to scaling can be modeled by characterizing the bubble size distribution in terms of the average and critical bubble radii, the latter of which demarcates growing versus shrinking bubbles [28]. This leads to average growth as

$$R(t) = [\mathcal{D}(t - t_o) + (R_o - \delta)^{1/\beta}]^\beta + \delta \quad (2)$$

where  $\delta$  emerges as a signed length reflecting the difference in width of the bubble size distribution at  $t_o$  from that in the scaling state [28]. Fits to this form allow testing of exponent predictions, and extraction of effective exponents, with minimal error due to transients.

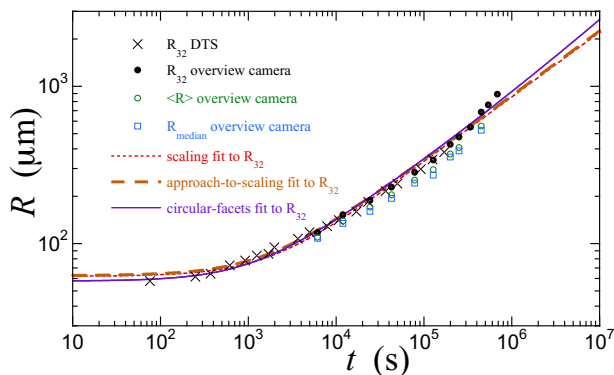


FIG. 1. Radius versus time data for a foam with 40% liquid from Fig. 10 of Ref. [24]. The crosses and solid circles are for  $R_{32} = \langle R^3 \rangle / \langle R^2 \rangle$ , respectively obtained from diffuse transmission spectroscopy (DTS) and the overview camera. The open circles and squares are for the average and median radii, respectively. The dotted and dashed curves represent fits to the combined  $R_{32}$  data to Eq. (1) and Eq. (2), respectively. The resulting exponent values are collected in Fig. 4. The solid curve represents numerical integration of Eq. (4) using  $\ell = 30$  nm  $f = 0.036$ , per Fig. 4, starting from fixed initial conditions of  $R_{32}(10 \text{ s}) = 58 \mu\text{m}$ ; the proportionality constant was adjusted to  $21 \mu\text{m}^3/\text{s}$  to match the combined  $R_{32}$  data.

One way to treat data outside the extreme wet and dry limits is to use the exponent  $\beta$  as an adjustable fitting parameter to empirically describe the observed time evolution. This is illustrated in Fig. 3 of Ref. [20], Figs. 1 & 3 of Ref. [21], and Fig. 1 here. The latter is for a wet foam measured aboard the ISS [24], and includes fits to a measure of average bubble size,  $R_{32} = \langle R^3 \rangle / \langle R^2 \rangle$ . Average and median radii are also included for comparison, though  $R_{32}$  should be less sensitive to the possibility of small bubbles being missed in automated image analyses [24]. As seen, the three different radii are not quite proportionate at early times but may become so at later times - consistent with observation [25] that the bubble size distribution approaches a self-similar scaling state. The displayed fits to Eqs. (1-2) are reasonable, but not outstanding (the “circular facets fit”, discussed below, is slightly better). The exponents from such fits to the various radii have mutually-consistent values in the range  $0.38 < \beta < 0.41$  and an average uncertainty of  $\pm 0.04$ . This comparison across different but equally-acceptable fitting forms to various radii helps gauge the confidence with which effective exponents can be measured, regardless of unknown transients on approach to scaling.

To justify such exponent-fitting approaches, and show how even rough values of  $\beta$  can be understood physically in terms of key features of the bubble-packing structure that change with liquid content, I now leverage the border-crossing physics of Ref. [29]. There, diffusive fluxes in complex microstructures were accurately modeled by stratified approximations to the dissolved gas concentration field in between bubbles. For two nearly-

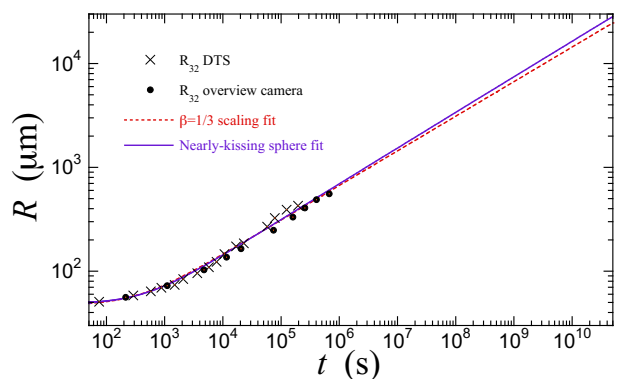


FIG. 2. Radius versus time for the wettest foam in Fig. 10 of Ref. [24], and fits to Eq. (1) (dotted) and Eq. (3) with  $\ell = 30$  nm (solid). The quality of fit for the latter is unchanged if  $\ell$  is varied across the range 20–40 nm or more. The  $x$  and  $y$  axes are respectively extended to span factors of  $10^9$  and  $10^3$  to emphasize the close similarity of the two fitting forms.

kissing spheres of similar radii  $r_1 \approx r_2 \approx R$  separated by  $\ell \ll R$ , Eq. (28) of Ref. [29] simplifies to approximately  $dR^3/dt \propto \ln(R/\ell)$  [30]. Separating variables and integrating gives the following prediction for the average growth law at the jamming transition:

$$t = t_o + \frac{1}{\mathcal{D}} \left[ \frac{R^3}{\ln(R/\ell)} - \frac{R_o^3}{\ln(R_o/\ell)} \right]. \quad (3)$$

While this cannot be inverted for  $R(t)$  and is not a pure power law, it is only logarithmically different from the  $\beta = 1/3$  scaling form of Eq. (1) for the dilute-bubble limit. Indeed, as shown in Fig. 2, these two forms compare indistinguishably well to the wettest foam data recently obtained aboard the ISS [23, 24]. More precise data, taken over an impracticably long duration, would be needed to discriminate between Eq. (3) and a pure  $1/3$  power law. Eq. (3), which holds for nearly-kissing spheres with  $\ell \ll R$ , thus explains the shocking Ref. [21] finding of  $\beta \rightarrow 1/3$  at the jamming transition.

The same border-crossing approach may now be used to calculate gas transfer rate between slightly jammed bubbles, which are nearly spherical and contact at nearly-circular films of radius  $\rho_f$  and thickness  $\ell$  satisfying  $\ell \ll \rho_f \ll R$ , as depicted in Fig. 3a for a suitably disordered packing (and in Refs. [31, 32] for crystalline packings). Note that  $\ell$  and  $R$  remain nearly constant while  $\rho_f$  shrinks to zero on approach to unjamming; thus,  $\rho_f$  is a crucial length scale for microstructure. Following Ref. [29] and using the sketch of Fig. 3b, the average volumetric growth rate is found by integrating the diffusive flux of dissolved gas between two contacting bubbles as  $dR^3/dt \propto \int_0^{\rho_f + aR} [D\Delta\phi/e(\rho)]\rho d\rho$  where the concentration difference  $\Delta\phi$  just outside the two bubbles is proportional to  $h\sigma/R$  as above,  $e(\rho)$  is the separation between the bubble interfaces at axial distance  $\rho$ , and  $aR$  with  $a = \mathcal{O}(1)$  imposes a cutoff beyond which there is little

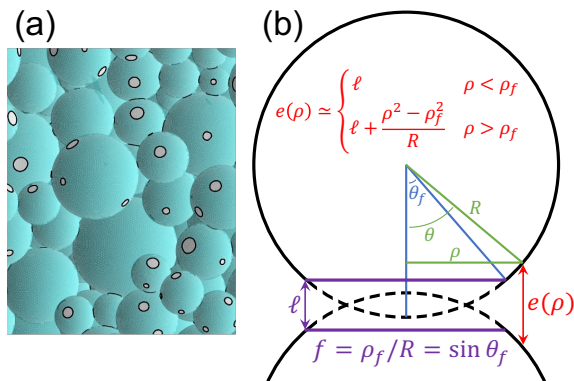


FIG. 3. (a) Close to unjamming, bubbles are nearly spherical and their contacts are nearly circular soap films of thickness  $\ell$  [33], such that  $\ell \ll \rho_f \ll R$  where  $\rho_f$  and  $R$  are the average film and bubble radii, respectively. (b) Therefore, the ratio  $f = \rho_f/R$  of film to bubble radii is small and the surface-surface separation  $e(\rho)$  versus axis distance  $\rho$  is well-approximated as displayed for the region where most gas transport occurs.

flux. As shown in Fig. 3b, the quantity  $e(\rho)$  is approximately  $\ell$  for  $\rho < \rho_f$  and  $\ell + (\rho^2 - \rho_f^2)/R$  for  $\rho > \rho_f$ . Defining the ratio of film to bubble radii as  $f = \rho_f/R$ , which is a small number set by distance to unjamming, and integrating, gives the average growth law as

$$\frac{dR^3}{dt} \propto \ln\left(\frac{R}{\ell}\right) + \frac{f^2 R}{\ell} \quad (4)$$

plus  $\ln(a)$ , which is dropped since  $a = \mathcal{O}(1)$  and  $\ell \ll R$ . The first term comes from the  $\rho > \rho_f$  portion of the integral, and leads to Eq. (3) at jamming where  $f = 0$ . The second term comes from the  $\rho < \rho_f$  portion of the integral, and accounts for gas flux across the thin film.

While Eq. (4) predicts average growth that is not a pure power law, it nevertheless provides insight for the variation of effective exponents,  $\beta$ , with liquid content. Since the two terms respectively give exponents of  $1/3$  and  $1/2$  if they were to act alone, I estimate  $\beta$  as the average of these values using the respective terms as weights:

$$\beta = \frac{\frac{1}{3} \ln\left(\frac{\bar{R}}{\ell}\right) + \frac{1}{2} \frac{f^2 \bar{R}}{\ell}}{\ln\left(\frac{\bar{R}}{\ell}\right) + \frac{f^2 \bar{R}}{\ell}} \quad (5)$$

where  $\bar{R}$  is the average bubble size throughout the duration of the observations. In typical experiments  $R$  grows by only a decade or so; therefore, one might take  $\bar{R}$  as the geometric average of the characteristic radius at the earliest and latest times. The expectation is that longer-duration growth data would be less power law-like and that results for  $\beta$  would depend on fitting range. A nice feature of Eq. (5) is that the ratio  $f = \rho_f/R$  of film to bubble radii is the only parameter relating to the bubble-scale microstructure that varies with liquid content; hence, it may be deduced from measurement of  $\beta$ ,

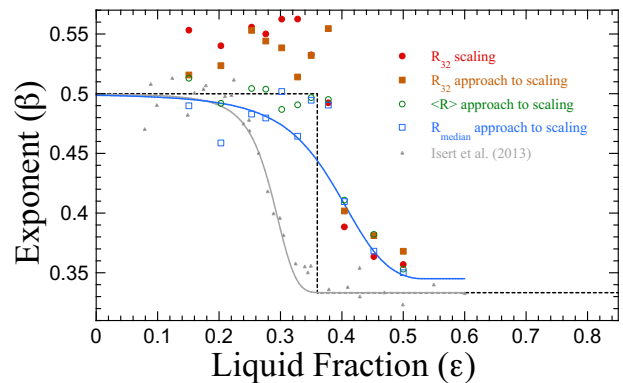


FIG. 4. Effective coarsening exponents versus liquid fraction. The solid circles and squares are from fits of Eqs. (1,2) to  $R_{32}$  data from Fig. 10 of Ref. [24], while the open circles and squares are from fits to average and median radii from the overview camera. The small triangles were extracted [36] from Fig. 4 of Isert *et al.* [21]. The dotted line segments are the step function  $1/2$  for  $\epsilon < 0.36$  and  $1/3$  for  $\epsilon > 0.36$ . The solid curves represent Eq. (5) for different functions  $f(\epsilon)$  chosen as described in the text in order to match the Ref. [21] and  $R_{\text{median}}$  data, respectively.

or it may be measured or modelled directly and used to predict  $\beta$ , if  $\bar{R}/\ell$  is known. While this treatment is intended for nearly unjammed foams, its range of applicability might be quite wide: Bubbles appear more spherical than polyhedral in images of foams as dry as even 8% liquid [20, 21, 24].

To use Eq. (5) for understanding experimental results, I first gather data from two sources. This includes published exponents from Ref. [21], where  $\bar{R} \approx 200$  nm; the bubbles of this system are relatively noncohesive, and have a film thickness of roughly  $\ell \approx 15$  nm [34]. It also includes exponents from my fits of Eqs. (1,2), per Fig. 1, to the growth of various radii extracted from ISS measurements [23, 24] where  $\bar{R} \approx 200$  nm, too; the bubbles of this system are noticeably cohesive and have a film thickness of about  $\ell \approx 30$  nm [25, 34, 35]. The various exponents are all plotted versus liquid fraction  $\epsilon$  in Fig. 4. With increasing wetness,  $\beta$  values for the noncohesive system decrease from around  $1/2$  to around  $1/3$  at random close packing [21]. For the second system,  $\beta$  values are considerably more scattered, crossing from around  $1/2$  to slightly above  $1/3$  though at a higher liquid fraction. This may be due to stronger bubble-bubble cohesion, which would pull bubbles into closer contact, and cause the ratio of film to bubble radii to be a nonzero constant,  $f_0$ , even in the wet limit.

Fixing  $\bar{R}/\ell$  for both systems per above, Eq. (5) may now be fit directly to  $\beta$  data by assuming the simplest piecewise form for the variation of  $f$  with  $\epsilon$  that falls smoothly to  $f_0$  at high liquid content:  $f(\epsilon) = f_0 + f_2(\epsilon - \epsilon_c)^2$  below  $\epsilon_c$  and  $f(\epsilon) = f_0$  above  $\epsilon_c$ . Fits give  $\{ f_0 \approx 0, f_2 = 3.7 \pm 1, \epsilon_c = 0.37 \pm 0.01 \}$  for the noncohesive

system and  $\{ f_0 = 0.010 \pm 0.003, f_2 = 1.4 \pm 0.4, \varepsilon_c = 0.53 \pm 0.02 \}$  for the median radius data for the cohesive system. Eq. (5) is plotted by solid curves in Fig. 4 for these sets of parameters, and is seen to match the data quite well. However, more and better exponent data near unjamming would permit a better test.

Circling back to the ISS radius versus time plot of Fig. 1, I now numerically integrate Eq. (4) growth law using  $\ell = 30$  nm and  $f(0.4) = 0.036$ , per the fit in the previous paragraph. Initial conditions are fixed as  $R_{32}(10\text{ s}) = 58\text{ }\mu\text{m}$ , and only the proportionality constant is adjusted in order to match the growth of the combined  $R_{32}$  data versus time. The agreement is slightly better than the scaling and approach-to-scaling power-law forms. This boosts confidence both in Eq. (4) and its use for estimating an effective exponent, Eq. (5), for non- power-law growth.

In conclusion, the success of Eqs. (3-5) for cohesive and noncohesive foams fill a void in the literature by providing physical insight and a general theoretical framework for modeling diffusive growth between the known extremes where  $\beta = 1/2$  and  $1/3$  hold. This approach is applicable to a broad range of phase-separating materials with analogous microstructure [1, 3], and opens myriad lines of further research. Besides more and better exponent data near unjamming, it would be interesting if the form found for  $f(\varepsilon)$  could be justified by combining ideas from the field of jamming with knowledge of how foam microstructure arises from surface tension and interfacial forces. This could be supplemented by incorporation of a contact angle between cohering bubbles, and variation of  $\ell$  with liquid content. Another issue could be to account for gas transfer between neighboring bubbles that are not in actual contact, by averaging over a distribution of separations ranging upwards from the film thickness. The same border-crossing approach can also be taken near the dry limit, where the flux through a nearly-polygonal film of area  $A$  and perimeter  $P$  is proportional to  $A/\ell + (3\pi/2)\sqrt{r/\ell}P$  where  $r \sim \sqrt{\varepsilon}R$  is the Plateau border curvature [29]; this gives an average growth law of  $dR^3/dt = a(R/\ell) + b\sqrt{\varepsilon^{1/2}R/\ell}$  where  $\{a, b\}$  are independent of  $\varepsilon$ . As per Eq. (5), the corresponding growth exponent is the average of  $1/2$  and  $2/5$  using these two terms as weights. All these predictions for average growth rates and effective exponents could be tested by incorporating border-crossing expressions for diffusive gas flux into simulations of accurate bubble-scale microstructure for wet foams, *e.g.* by extension of Refs. [31, 32, 37–40].

I thank Reinhard Höhler and Dominique Langevin for helpful discussions; Sylvie Cohen-Addad and Olivier Pitois for assistance with ISS data from the Foam-C project of ESA [23, 24]; and Andy Kraynik for permission to use Fig. 3a [33]. My work was supported by NASA via grant number 80NSSC21K0898.

- 
- [1] W. W. Mullins, “The statistical self-similarity hypothesis in grain growth and particle coarsening,” *Journal of Applied Physics* **59**, 1341–1349 (1986).
  - [2] P. W. Voorhees, “The Theory of Ostwald Ripening,” *Journal of Statistical Physics* **38**, 231–252 (1985).
  - [3] J. Stavans, “The evolution of cellular structures,” *Rep. Prog. Phys.* **56**, 733–789 (1993).
  - [4] J. von Neumann, in *Metal Interfaces* (American Society for Metals, Cleveland, 1952) pp. 108–110.
  - [5] W. W. Mullins, “Two-dimensional motion of idealized grain boundaries,” *Journal of Applied Physics* **27**, 900–904 (1956).
  - [6] D. Weaire and S. Hutzler, *The Physics of Foams* (Oxford University Press, 1999).
  - [7] R. D. MacPherson and D. J. Srolovitz, “The von Neumann relation generalized to coarsening of three-dimensional microstructures,” *Nature* **446**, 1053 (2007).
  - [8] P. Stevenson, “Inter-bubble gas diffusion in liquid foam,” *Current Opinion in Colloid & Interface Science* **15**, 374–381 (2010).
  - [9] I. Cantat, S. Cohen-Addad, F. Elias, F. Graner, R. Höhler, O. Pitois, F. Rouyer, and A. Saint-Jalmes, *Foams: Structure and Dynamics* (Oxford University Press, 2013).
  - [10] D. Langevin, *Emulsions, Microemulsions and Foams* (Springer International Publishing, 2020).
  - [11] I. M. Lifshitz and V. V. Slyozov, “The kinetics of precipitation from supersaturated solid solutions,” *Journal of Physics and Chemistry of Solids* **19**, 35–50 (1961).
  - [12] C. Wagner, “Theorie der alterung von niederschlagen durch umlosen (Ostwald-reifung),” *Zeitschrift fur Elektrochemie* **65**, 581–591 (1961).
  - [13] P. Taylor, “Ostwald ripening in emulsions,” *Advances in Colloid and Interface Science* **75**, 107–163 (1998).
  - [14] B.A. Pletcher, K.G. Wang, and M.E. Glicksman, “Experimental, computational and theoretical studies of delta’ phase coarsening in Al-Li alloys,” *Acta Materialia* **60**, 5803–5817 (2012).
  - [15] S. Hutzler and D. Weaire, “Foam coarsening under forced drainage,” *Philos. Mag. Lett.* **80**, 419 (2000).
  - [16] S. Hilgenfeldt, S. A. Koehler, and H. A. Stone, “Dynamics of coarsening foams: Accelerated and self-limiting drainage,” *Phys. Rev. Lett.* **86**, 4704 (2001).
  - [17] K. Feitosa and D. J. Durian, “Gas and liquid transport in steady-state aqueous foam,” *Eur. Phys. J. E* **26**, 309 (2008).
  - [18] I. Fortuna, G. L. Thomas, R. M. C. de Almeida, and F. Graner, “Growth laws and self-similar growth regimes of coarsening two-dimensional foams: Transition from dry to wet limits,” *Phys. Rev. Lett.* **108**, 248301 (2012).
  - [19] G. L. Thomas, J. M. Belmonte, F. Graner, J. A. Glazer, and R. M. C. de Almeida, “3d simulations of wet foam coarsening evidence a self similar growth regime,” *Colloids and Surfaces A: Physicochemical and Engineering Aspects* **473**, 109–114 (2015).
  - [20] D. J. Durian, D. A. Weitz, and D. J. Pine, “Scaling behavior in shaving cream,” *Phys. Rev. A* **44**, R7902 (1991).
  - [21] N. Isert, G. Maret, and C. M. Aegerter, “Coarsening dynamics of three-dimensional levitated foams: From wet to dry,” *The European Physical Journal E* **36**, 116 (2013).
  - [22] H. Yan, K.G. Wang, and M.E. Glicksman, “Microstruc-

- tural coarsening in dense binary systems,” *Acta Materialia* **233**, 117964 (2022).
- [23] P. Born, M. Braibanti, L. Cristofolini, S. Cohen-Addad, D. J. Durian, S. U. Egelhaaf, M. A. Escobedo-Sánchez, R. Höhler, T. D. Karapantsios, D. Langevin, L. Liggieri, M. Pasquet, E. Rio, A. Salonen, M. Schröter, M. Sperl, R. Sütterlin, and A. B. Zuccolotto-Bernez, “Soft matter dynamics: A versatile microgravity platform to study dynamics in soft matter,” *Review of Scientific Instruments* **92**, 124503 (2021).
- [24] M. Pasquet, N. Galvani, O. Pitois, S. Cohen-Addad, R. Höhler, A.T. Chieco, S. Dillavou, J. M. Hanlan, D. J. Durian, E. Rio, A. Salonen, and D. Langevin, “Aqueous foams in microgravity, measuring bubble sizes,” *Comptes Rendus Mécanique* **351**, 1–23 (2023).
- [25] N. Galvani, M. Pasquet, A. Mukherjee, A. Requier, S. Cohen-Addad, O. Pitois, R. Höhler, E. Rio, A. Salonen, D. J. Durian, and D. Langevin, “Hierarchical bubble size distributions in coarsening wet liquid foams,” arXiv:2304.11543 (2023).
- [26] A. T. Chieco, J. P. Sethna, and D. J. Durian, “Average evolution and size-topology relations for coarsening 2d dry foams,” *Frontiers in Soft Matter* **2** (2022), <https://doi.org/10.3389/frsfm.2022.941811>.
- [27] The exact factor for ideal dry 2d foams is based on von Neumann’s law and statistical self-similarity. The factor for ideal dry 3d foams based similarly on MacPherson and Srolovitz’s law and statistical self-similarity is unknown.
- [28] A. T. Chieco and D. J. Durian, “A simply solvable model capturing the approach to statistical self-similarity for the diffusive coarsening of bubbles, droplets, and grains,” arXiv:2303.09612 (2023).
- [29] C. D. Schimming and D. J. Durian, “Border-crossing model for the diffusive coarsening of two-dimensional and quasi-two-dimensional wet foams,” *Phys. Rev. E* **96**, 032805 (2017).
- [30] To obtain this approximation from Eq. (28) of Schimming and Durian I use  $I_s \propto dR^3/dt$  and  $\Delta\phi \propto 1/R$ , since  $a$  and  $c$  can be dropped and since  $\log(bR/\ell) \approx \log(R/\ell)$ .
- [31] Reinhard Höhler and Denis Weaire, “Can liquid foams and emulsions be modeled as packings of soft elastic particles?” *Advances in Colloid and Interface Science* **263**, 19–37 (2019).
- [32] S. Hutzler, F. F. Dunne, A. M. Kraynik, and D. Weaire, “The energy of fcc and hcp foams,” *Soft Matter* **16**, 8262–8271 (2020).
- [33] Surface Evolver simulation of a polydisperse foam at liquid fraction  $\epsilon = 0.30$ , presented by A.M. Kraynik at EU-Foam 2020 (unpublished).
- [34] V. Bergeron and C. J. Radke, “Equilibrium measurements of oscillatory disjoining pressures in aqueous foam films,” *Langmuir* **8**, 3020–3026 (1992).
- [35] M. Pasquet, N. Galvani, A. Requier, S. Cohen-Addad, R. Höhler, O. Pitois, E. Rio, A. Salonen, and D. Langevin, “Coarsening transitions of wet liquid foams under microgravity conditions,” arXiv:2304.11206 (2023).
- [36] <https://automeris.io/WebPlotDigitizer/>.
- [37] J. A. Glazier, M. P. Anderson, and G. S. Grest, “Coarsening in the 2-dimensional soap froth and the large-Q Potts-model - A detailed comparison,” *Philos. Mag. B* **62**, 615–645 (1990).
- [38] K. A. Brakke, “The surface evolver,” *Experimental Mathematics* **1**, 141–165 (1992).
- [39] E. A. Lazar, J. K. Mason, R. D. MacPherson, and D. J. Srolovitz, “A more accurate three-dimensional grain growth algorithm,” *Acta Materialia* **59**, 6837–6847 (2011).
- [40] Y. Kim, M.-C. Lai, C. S. Peskin, and Y. Seol, “Numerical simulations of three-dimensional foam by the immersed boundary method,” *Journal of Computational Physics* **269**, 1–21 (2014).